Université de Mons
Faculté Polytechnique – Service de Mécanique Rationnelle, Dynamique et Vibrations
31, Bld Dolez - B-7000 MONS (Belgique)
065/37 42 15 – georges.kouroussis@umons.ac.be

L. Ben Fekih, O. Verlinden, G. Kouroussis, Mechanical characterization of E-glass laminates under large bending, *Composite Structures*, 255, 112892, 2021

Composite Structures 255 (2021) 112892

Contents lists available at ScienceDirect

Composite Structures

journal homepage: www.elsevier.com/locate/compstruct

Mechanical characterization of E-glass laminates under large bending

Lassaad Ben Fekih [a,*], Olivier Verlinden [a], Georges Kouroussis [a]

[a] Department of Theoretical Mechanics, Dynamics, and Vibrations, University of Mons, Place du Parc 20, 7000 Mons, Belgium

ARTICLE INFO

Keywords:
E-glass laminates
Novel test specimens
Large bending
Lamina properties

ABSTRACT

This study focuses on epoxy fiberglass (E-glass) laminates used as printed circuit boards, more particularly as flexible substrates in fracture assemblies for the test of attachments of electronic components such as solder and adhesive joints. Breaking these joints often requires large bending of E-glass substrates. Such circumstances have not been investigated before. In fact, most research focused on the linear elastic behaviour of E-glass. Therefore, static large bending tests were conducted on instrumented cantilever and square plates. Test data consisting of pull force and strain versus deflection curves revealed that the behaviour of E-glass laminates is overall non-linear-elastic. Next, the correlation between simulated and measured structural responses of test prototypes led to determining E-glass lamina properties applicable upon large bending.

1. Introduction

Epoxy fibreglass (E-glass) laminates are widely used as flexible supports in test vehicles to emulate actual Printed Circuit Boards (PCBs). In connection with space applications, E-glass laminates offer benefits of lower cost and high resilience compared to PCBs usually made of polymide and copper materials. Test vehicles are involved in the mechanical qualification of solder and adhesive attachments of electronic components. In fact, the harsh vibratory environment of the space launch causes PCB bending, which highly loads such joints. The qualification phase entails fracture tests where E-glass supports are prone to exhibit large deflections to possibly break the attachment under test. The present study aims at exploring the mechanical behaviour of E-glass laminates under large bending and, after that, identifying their mechanical properties.

From an experimental point of view, static and modal testing methods are mostly reported in the literature for the characterization of laminated composites. Static testing is supplied with standards such as ASTM-D882 and ISO-527 standard or IPC-TM-650, which has numerous downsides. Firstly, Ullah et al. [1] emitted that the mechanical properties of carbon fabric-reinforced polymer composites obtained by tensile tests are lower than ones derived from bending tests. Behind, there is a difference in stress distributions: while glass fibres stretch uniformly under tension causing the weakest fibre to fail first, it is the top/bottom fibres that are utmost stressed under convex/concave bending. Secondly, tensile tests suffer from a matter of generality referred to as mesh-size effect. According to Ref. [2], the strength and elastic moduli decrease with increasing thickness/volume due to the presence of larger defects. As regards bending tests, a matter of completeness concerns 3-point and 4-point bend fixtures disclosed in [3,4] standards which unable to emulate the biaxial bending of real electronic boards. Together, tension and bending tests suffer from a difficult characterization of out-of-plane properties of laminated composites. Fuchs et al. [5] handled this challenge through micro-mechanics using a combination of experiments and mean-field homogenization computation. The modal analysis hinges on identifying the mechanical properties of tested components through the update of an equivalent mathematical model. Paepegem and Degrieck [6] applied the modal approach to determine the mechanical properties of E-glass using vibrating cantilever beams. Their updating method was adopted by Sol et al. [7], who updated the anisotropic rigidity terms of fibre-reinforced composites through the resonant frequencies of freely suspended rectangular plates. This procedure provides better accuracy in yielding diagonal rigidity terms of the material. Conversely, off-diagonal terms suffer from a weak dependency on the resonance frequencies due to the Poisson's ratio. As a result, the updated mechanical properties can be inconsistent. This is obvious from the Poisson's ratio estimated at 0.49 and 0.51 in Ref. [8] with isotropic and orthotropic behaviours assigned to polyimide PCB, against 0.12 recommended for this material in Ref. [9]. To cite one, the merit of the modal approach lies to its rapid assessment of the mechanical properties of complex-geometry structures such as ones including stiffening ribs [10]. In addition, it is worth mentioning that the modal analysis

* Corresponding author.
E-mail address: lassaad.benfekih@umons.ac.be (L. Ben Fekih).

https://doi.org/10.1016/j.compstruct.2020.112892
Received 4 February 2020; Revised 19 June 2020; Accepted 24 August 2020
Available online 1 September 2020

operates on the linear response of the material invoking small deformations.

On the one hand, it appears that the aforementioned research investigated the linear elastic response of laminated composites. This is attributed to the design under the requirement of elasticity, which facilitates the numerical and analytical structural calculations, and to the fact that vibrations are unlikely to induce large PCB deflections in real applications. On the other hand, Dahale et al. [11] provided evidence for the nonlinear elastic behaviour of E-glass laminates under excessive tension loading. Similar findings were obtained in Ref. [12] under off-axis tension. The authors scrutinized existing macroscopic and microscopic approaches used to predict the nonlinear behaviour of laminated composites. A three-parameter orthotropic plasticity model was demonstrated suitable for E-glass laminates, following a macroscopic approach. So far, no study was found to put evidence in the nonlinear behaviour of E-glass under large bending, which corroborates the need to explore the behaviour of E-glass under such conditions, and confirm the essence (elastic, plastic) of any nonlinearity. The present work proposes novel test prototypes for this purpose. Unlike standard test arrangements, which dispose of established analytical forms for the identification of the mechanical properties of laminates directly from test data, here, the use of novel test prototypes obliges to rely on the correlation between simulated and measured structural responses of tested specimens. Accordingly, this suggests developing accurate numerical models for test prototypes.

From a numerical point of view, a substantial task consists in modelling the E-glass laminate either as a stack of individual laminae or as a single-layer. Know that the single-layer approach comes with reduced number of governing equations and involves fewer parameters compared to the layered approach [13]. The relationship between (strains, curvatures) and (tractions, bending moments) of laminates can rely either on the classical laminate plate theory (CLPT) or on the first-order shear deformation theory (FSDT). Abrate and Di Sciuva [14] stated CLPT pitfalls such as (1) the inextensibility in the transverse direction with a transverse normal strain, ε_z, equal to 0, (2) line segments that are perpendicular to the reference surface remain straight, and (3) line segments normal to the reference surface that remain perpendicular meaning that transverse shear strains, ε_{lz} and ε_{cz}, equal to zero. More readings on CLPT drawbacks could be found in [15,16]. The FSDT permits to address pitfalls (2) and (3) and accounts for the transverse shear deformations as outlined in [13,17]. Besides, the FSDT requires less computational effort relative to the CLPT as the shape function of FSDT-based elements should only satisfy C^0 continuity [17]. The background of FSDT relative to laminates is fully detailed in Appendix A. This manuscript is organized as follows: the second section reports static uniaxial and biaxial bending tests using cantilever and square E-glass specimens, respectively. The third section deals with the finite element (FE) modelling of both test prototypes and the behaviour of E-glass material. The fourth section includes sensitivity analyses delineating the dependency of models' output data on the mechanical properties of E-glass. Outcomes of sensitivity studies helped devise a numerical/experimental procedure for the identification of E-glass mechanical properties outlined in the last section of this work.

2. Experimental procedure

2.1. Uniaxial bending test

2.1.1. Specimen preparation and test procedure

The uniaxial bending arrangement consists of a 120 mm long, 20 mm wide, and 2 mm thick E-glass specimen fastened against a rigid mounting support made of aluminium. The specimen free end is connected to a force cell attached to a universal Instron 4505 machine (Fig. 1a) using a hinge joint, adaptation parts, and a universal joint. An exploded view of the whole test prototype is depicted in Fig. 1b. The center distance between the rotation axes of the hinge and universal joints should fit the workspace and minimize as much as possible the longitudinal in-plane tension to preclude specimen slippage. A center distance of 130 mm guarantees the slightest angular deviation worth $\pm 6^\circ$ for a maximum specimen deflection Z of 45 mm. The E-glass fabric is composed of fibreglass warp and weft yarns aligned at lengthwise and crosswise directions, respectively. The fact that warps are finer than wefts permitted to distinguish them visually, thus, prepared the measurement of E-glass crosswise strain, ε_c. In practice, Kyowa brand KFRP-2–120-C1-9 strain gage placed at 17 mm from the clamped specimen edge (Fig. 2) provided ε_c at the mid-longitudinal axis of the specimen. Other measurements consist of the cross-head displacement, Z, and the pull-up force, F, measured by a 5 kN load cell. A voltage input module NI-9202 recorded Z and F,

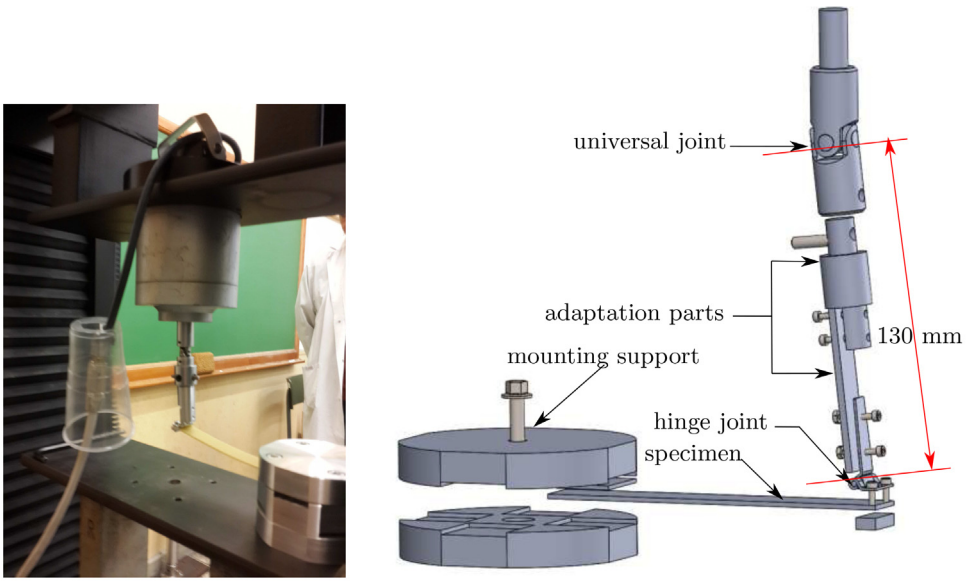

Fig. 1. Uniaxial bending prototype: (a) Real view, (b) Exploded view.

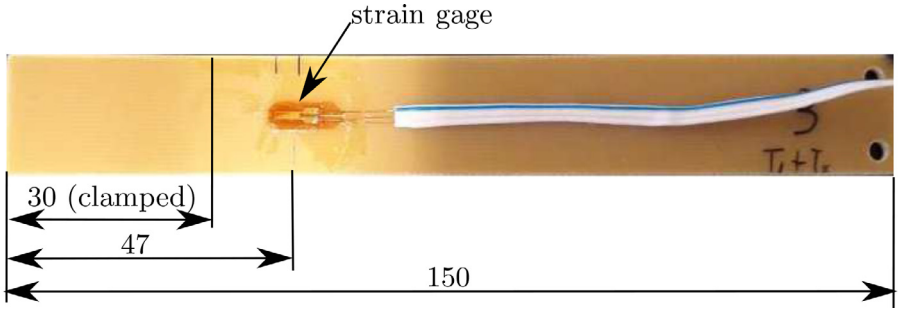

Fig. 2. Instrumented cantilever E-glass specimen.

while a NI-9237 strain bridge module recorded ε_c. The E-glass specimen was pulled up along its out-of-plane direction, as illustrated in Fig. 1. ISO-95 25217:2009 [18] recommends using a cross-head speed in 1–5 mm/min range when testing fibre-reinforced composites. Presently, tested specimens were subjected to a 1 mm/min cross-head speed up to $Z = 45$ mm at room temperature.

2.1.2. Uniaxial bending test data

The notation SPX-u refers to an E-glass specimen tested in uniaxial bending with "X" place holder indicating specimen number. Static bending tests were conducted on specimens SP1-u and SP2-u. SP1-u incurred a hysteresis loop: it was loaded for Z ranging between 0 and 25 mm, unloaded from 25 mm to -25 mm, and finally reloaded from -25 mm to 25 mm. This test attempted to verify the plastic deformation of the E-glass laminate through hysteresis loss. As a result, the evolution of F versus Z, or $Z-F$ curve, exhibited no significant hysteresis loss, as appears in Fig. 3a. SP2-u was bent up from 0 to 45 mm. Its corresponding $Z-F$ curve is illustrated in Fig. 3b. It reproduces a perfect agreement with the SP1-u $Z-F$ curve, which asserts the reproducibility of the test procedure. Besides, SP2-u testing provided the evolution of ε_c versus Z, as illustrated in Fig. 3c. Both $Z-F$ and $Z-\varepsilon_c$ curves permit to delimit the interval of linear elasticity of SP2-u by the detection of a 1% relative error between fit lines and experimental curves. In this way, the elastic limit of the E-glass

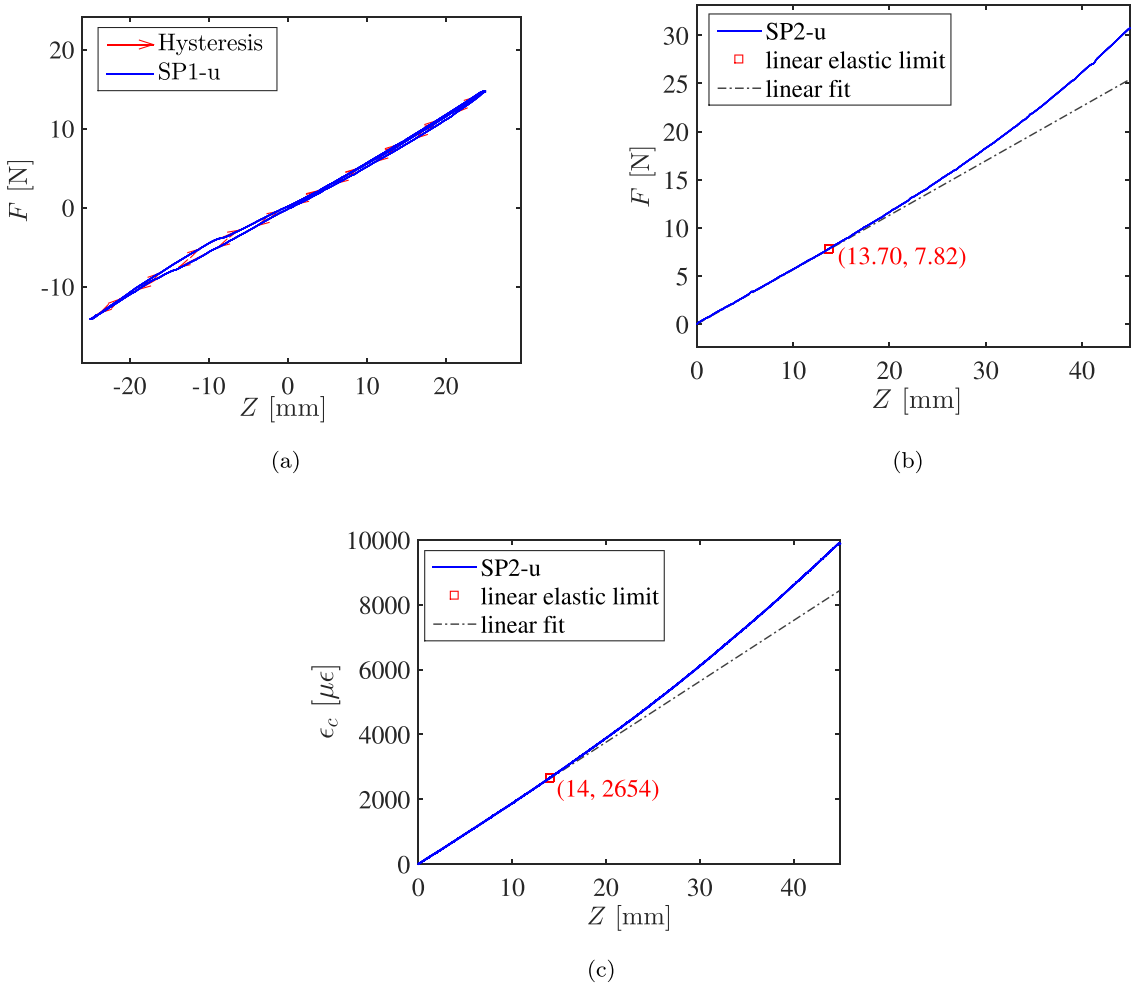

Fig. 3. Structural responses of E-glass specimens under uniaxial bending: (a) $Z-F$ curve of SP1-u, (b) $Z-F$ curve of SP2-u, and (c) $Z-\varepsilon_c$ curve of SP2-u.

specimen was established at $Z = 13.85$ mm on average from $Z - F$ and $Z - \varepsilon_c$, and ε_c at 2645 $\mu\varepsilon$ based on $Z - \varepsilon_c$. Such a finding could be of great interest to the design with a constraint on the elasticity.

2.2. Biaxial bending test

2.2.1. Specimen preparation and test procedure

The biaxial bending arrangement consists of a $150 \times 150 \times 1.85$ mm^3 E-glass specimen secured to fixed aluminium support by a set of fasteners from holes drilled at its corners. The fasteners consist of M3 bolts and nuts, 6.95 mm diameter washers and spacers of 10 mm diameter and height. Two steel blocks grip the two sides of the test specimen using an M3 tightening bolt through a hole drilled in. A ball joint put between the upper steel block and the testing frame ensures the compensation of any vertical misalignment. When subjected to cross-head displacement, the specimen exhibited a biaxial bending (Fig. 4). Measurements include Z and F as well as the lengthwise, crosswise, and diagonal strain components, denoted by ε_l, ε_c, and ε_d, respectively. Strain measurements emanate from Kyowa KFRP-2-120-D22-9 rosette placed at the backplane of the E-glass specimen outside the clamped region, as shown in Fig. 5. The biaxial bending test onsets with a manual pre-positioning of the upper grip of the testing frame to counteract the weight of the test prototype then to assign all measurements to zero. A number of three specimens were tested at a cross-head speed of 1 mm/min. All tested specimens sustained a deflection ramping up to 13 mm.

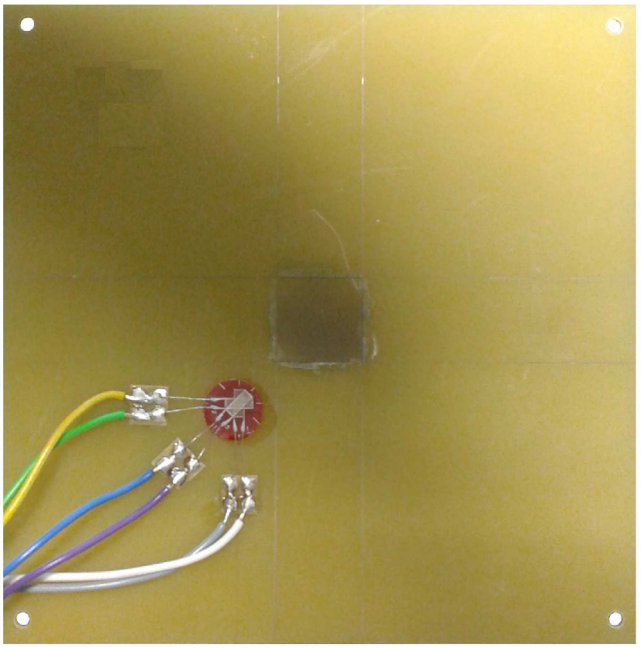

Fig. 5. Instrumented square E-glass specimen.

2.2.2. Biaxial bending test data

The structural responses of E-glass specimens under biaxial bending are illustrated in Fig. 6. Looking at $Z - \varepsilon_l$ and $Z - \varepsilon_c$ lays out the anisotropic behaviour of the E-glass material. The degree of anisotropy, obtained from the ratio of ε_c per ε_l, ranges between 1.1 and 1.4, which is deemed slight to moderate. Importantly, the specimen response splits into three regions. A first linear elastic region ranges from the origin to ($Z = 2.79 \pm 0.78$ mm – $F = 176$ N – $\varepsilon_l = 652$ $\mu\varepsilon$ – $\varepsilon_c = 787$ $\mu\varepsilon$ – $\varepsilon_c = 478$ $\mu\varepsilon$), worth 760 $\mu\varepsilon$ of maximum principal in-plane specimen strain. A second region starts from the end of the first region and extends to ($Z = 10.03 \pm 0.70$ mm – $F = 544$ N – $\varepsilon_l = 1361$ $\mu\varepsilon$ – $\varepsilon_c = 1779$ $\mu\varepsilon$ – $\varepsilon_c = 1329$ $\mu\varepsilon$). This behaviour can arise from a geometric nonlinearity

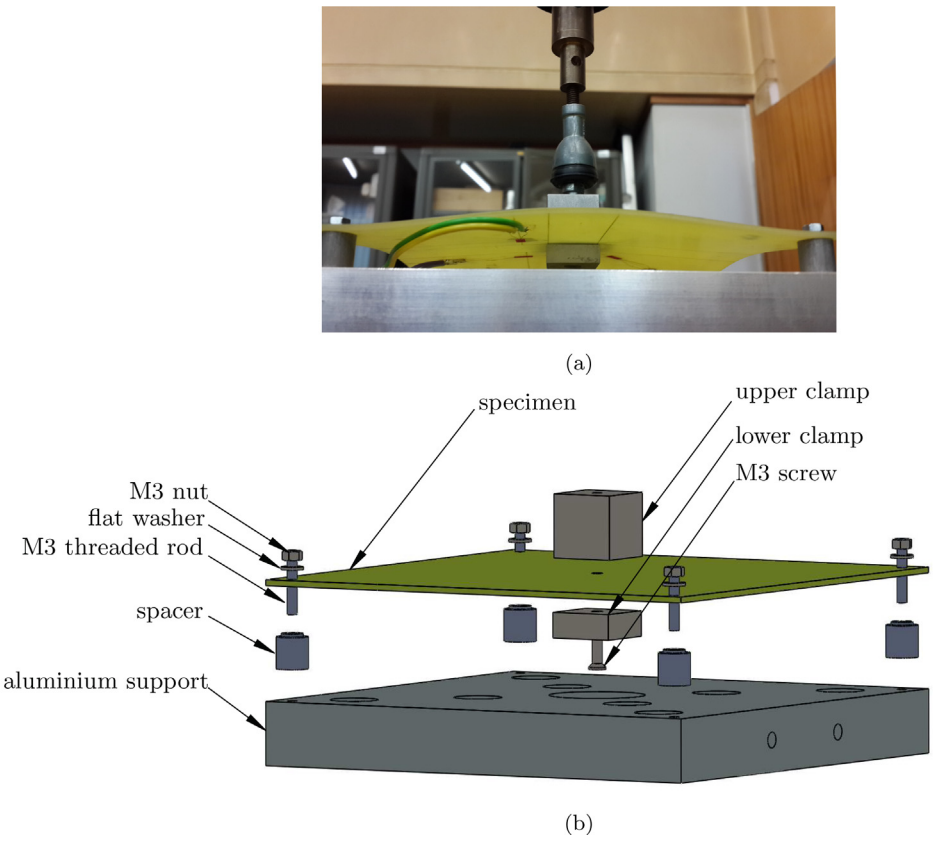

Fig. 4. Biaxial bending prototype: (a) Real view, (b) Exploded view.

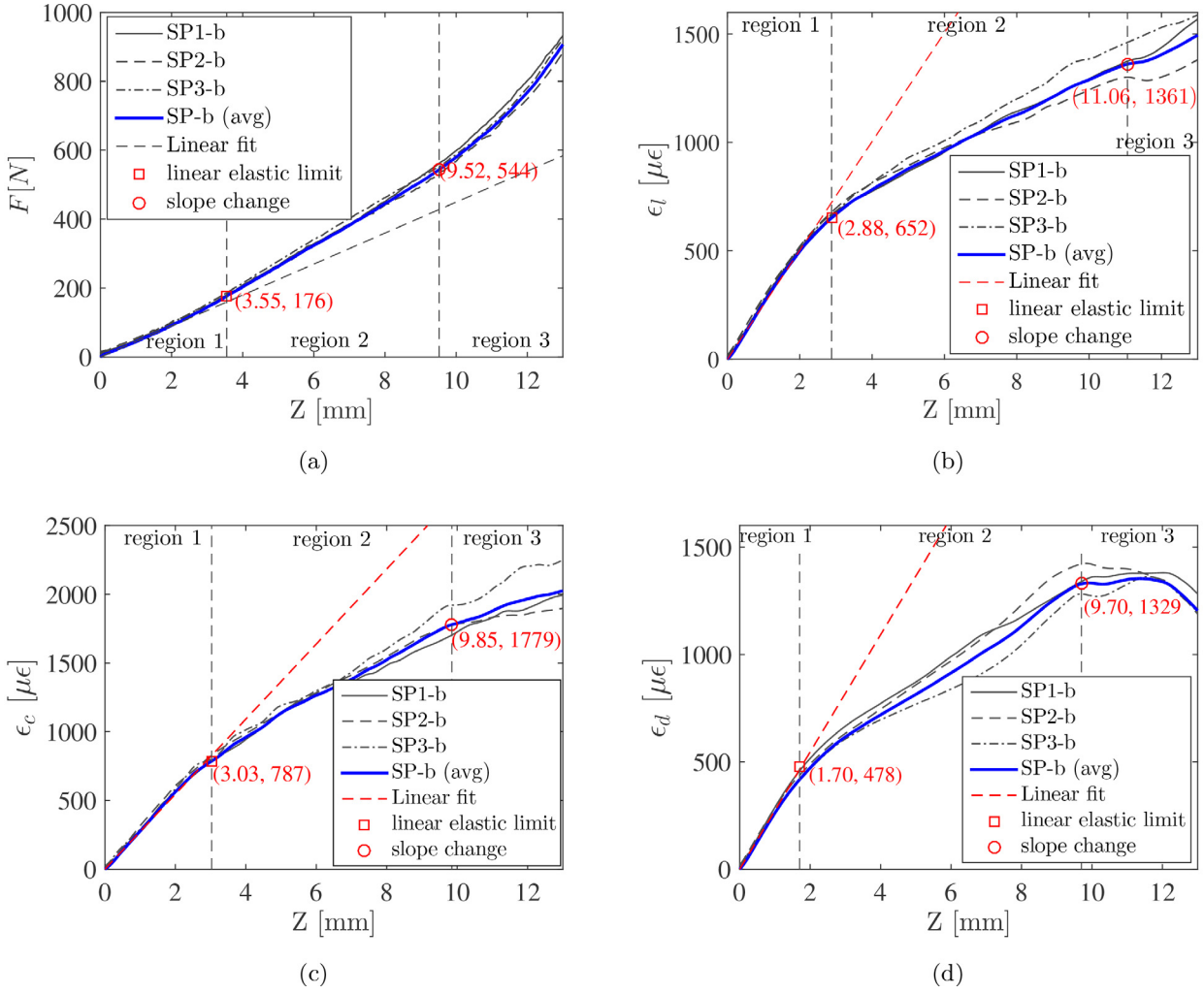

Fig. 6. Structural responses of E-glass specimens under biaxial bending: (a) Applied load, (b) E-glass backplane lengthwise strain, (c) E-glass backplane diagonal strain, and (d) E-glass backplane crosswise strain.

due to large bending or/and from material hardening. When releasing the specimen, all strain components return to zero. Thus, the assumption of geometric non-linearity is retained over material hardening. A third region exhibited an accentuated E-glass laminate stiffening apparent from the increasing pulling force and decreasing strains. This third zone is delimited, with caution at this stage, by slope deviation points indicated on $Z-F$ and $Z-\varepsilon_d$ curves. The rapid change of the specimen stiffness in region 3 will be investigated next.

3. Finite element modelling of test prototypes

The FE modelling of test prototypes is needed for the generation of simulated counterparts of experimental data following the approach indicated in Fig. 7. This section sketches out the preparation and validation of these models. The next section includes sensitivity studies invoked to figure out the dependency between models' outputs on the mechanical properties of the E-glass laminate, which

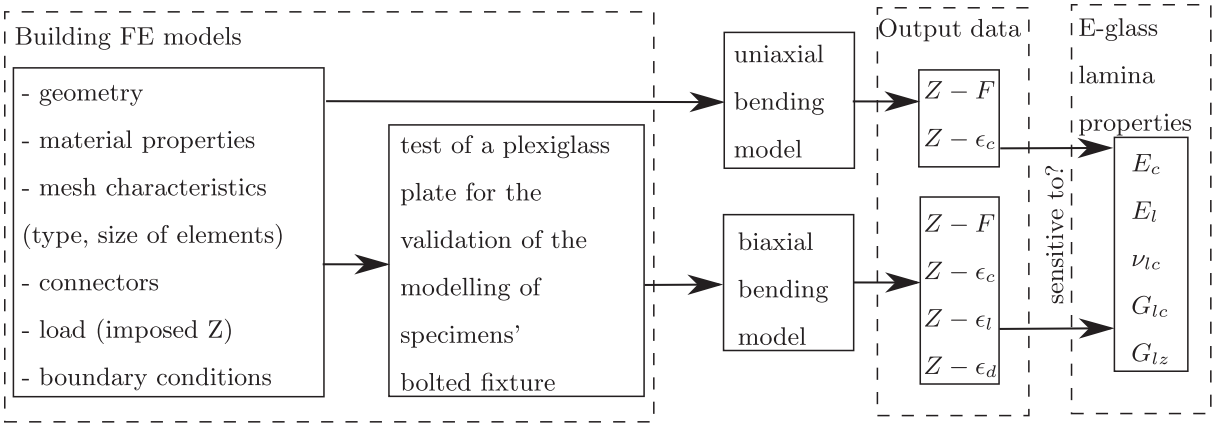

Fig. 7. Flowchart outlining the rationale of the FE modelling of test prototypes.

guides to establish a relevant experimental–numerical updating strategy.

3.1. Laminates modelling

The E-glass plate was modelled under Abaqus FE commercial Software using a single layer of shell elements, which are preferred over solid elements since they permit to avoid membrane and shear locking [19]. Abaqus supports conventional and continuum shell elements relying on FSDT and CLPT, respectively [20]. Conventional S4 four-node shell elements were chosen, similarly to many studies [21]. It is worth noting that S4 elements incorporate full integration, which, compared to reduced integration, circumvents spurious zero strain energy modes, so gains accuracy. Besides, Simpson integration was preferred to Gauss integration since it considers integration points at the top and bottom surfaces of the E-glass laminate, which avoids averaging results at such output locations. The authors realized that the convergence of the results requires at least five integration points with Simpson integration. Furthermore, the need for simulating large bending of the test specimen dictated the activation of the non-linear geometry option under Abaqus.

3.2. Uniaxial bending model

The degrees of freedom of the cantilever specimen were locked over 30 mm in length, as shown in Fig. 8a. Discrete rigid wires modelled the intermediate bar and the arm link between the universal joint and the force cell. In Fig. 8a, the reference point labelled “RP” defines the position of each wire. Abaqus built-in connectors modelled the kinematic joints: a hinge connector was interposed between the free end of the specimen along 12 mm (zone in grey in Fig. 8b) and the bottom of the intermediate bar, while a universal connector linked the top of the intermediate bar to the force cell. Lastly, a prismatic joint was connected to the force cell to ensure vertical displacement up to 45 mm. An element size of 1 mm was overall adopted, for which force and strain results begin to stabilize.

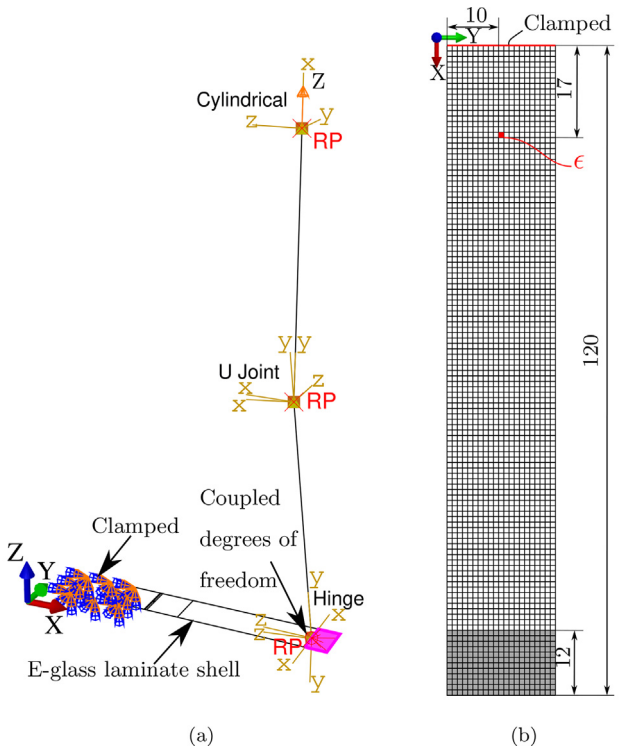

Fig. 8. Uniaxial bending model: (a) Loads and BCs (b) Geometry and mesh details (ϵ refers to the element where the E-glass strain is retrieved).

3.3. Biaxial bending model

Contrary to the uniaxial bending model, the E-glass unknown mechanical properties complicates the validation of boundary conditions (BC)s of the biaxial arrangement. The major difficulty lies in modelling contact properties between joined parts with an unquantified (slight) tightening torque applied on fixture bolts. Such a torque produces an axial force in bolts, referring to as preload force. It seems important to evaluate the effect of such a preload force on outputs of the biaxial prototype. As a solution, it is proposed to validate the BCs of this model on plexiglass XT material. Contrary to the E-glass material, the mechanical properties of the plexiglass are known (Table 1). Said validation relies on matching between measured and simulated $Z-F$ curves of a $150 \times 150 \times 3\ \text{mm}^3$ plexiglass plate. A full biaxial model is developed as depicted in Fig. 9a, where the sets of fasteners (nut + washer + threaded rod + spacer) are physically represented and all contacts modelled using a finite surface-to-surface sliding with normal and tangential behaviours based on “hard contact” and ”penalty” formulations, respectively. From now onwards, the square plexiglass/E-glass plate is meshed using structured quad-dominated elements of 1 mm edge size over the clamped region and the area surrounding the strain gage (highlighted in grey in Fig. 9b). Elsewhere, free quad shape elements of approximate 2 mm size apply. This mesh is the coarsest, yielding mesh-independent force and strain results. A vertical displacement, Z, is applied to a master reference point attached to a slave surface corresponding to the area of steel clamps.

Abaqus can account for the preload force in bolts through “bolt load” or “initial stress” approaches [23]. According to [23], the “bolt load” procures a better agreement between the simulated and test results in comparison with the “initiation stress” approach. This led to apply the “bolt load” approach following these steps:

- Step 0: application of BCs.
- Step 1: bolt preload applied on the two sides of the bolt middle surface + activation of contacts between interfaces.
- Step 2: fixing the bolt length [23] + application of a vertical displacement deemed as an external load.

Used as received (without lubricant), M3 bolts made of 8.8 stainless steel can sustain a preload force of 1866 N [24]. This maximum preload force is applied during the simulation of the plexiglass biaxial model with preload. As a result, Fig. 10a reveals an obvious discrepancy starting at $Z = 2$ mm between the measured and simulated $Z-F$ curves. Therefore, considering the preload should be disregarded. Without preload, the foregoing $Z-F$ curves agree perfectly until $Z = 7$ mm, as depicted in Fig. 10a. Fig. 10b shows that the plexiglass plate slips along x- and y-axes. The deviation point occurs when

Table 1
Mechanical properties of plexiglas XT [22].

Property	Young’s modulus	Poisson’s ratio	Flexural strength	Density
Unit	MPa		MPa	kg/m^3
Value	3300	0.37	105	1190

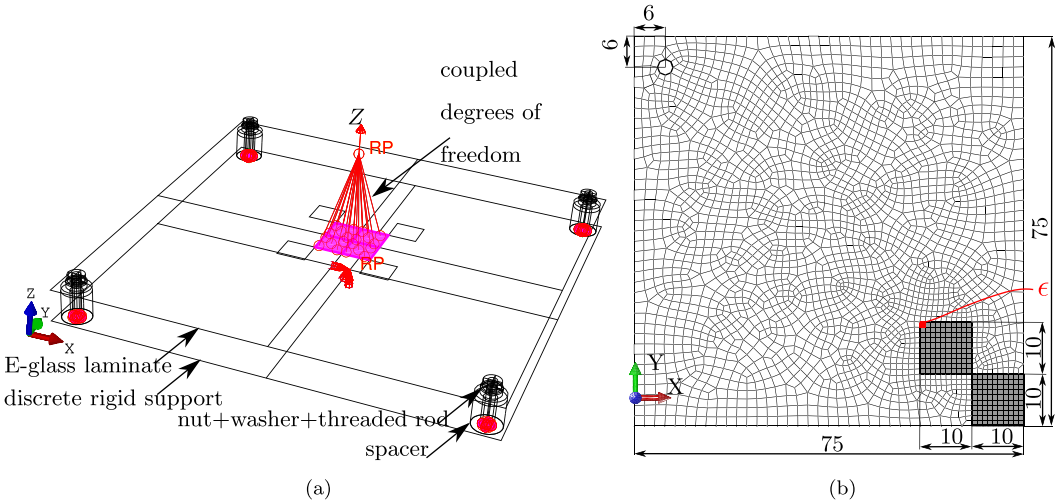

Fig. 9. Full biaxial bending model: (a) Loads and BCs, (b) Mesh and geometry details of quarter of the square E-glass plate.

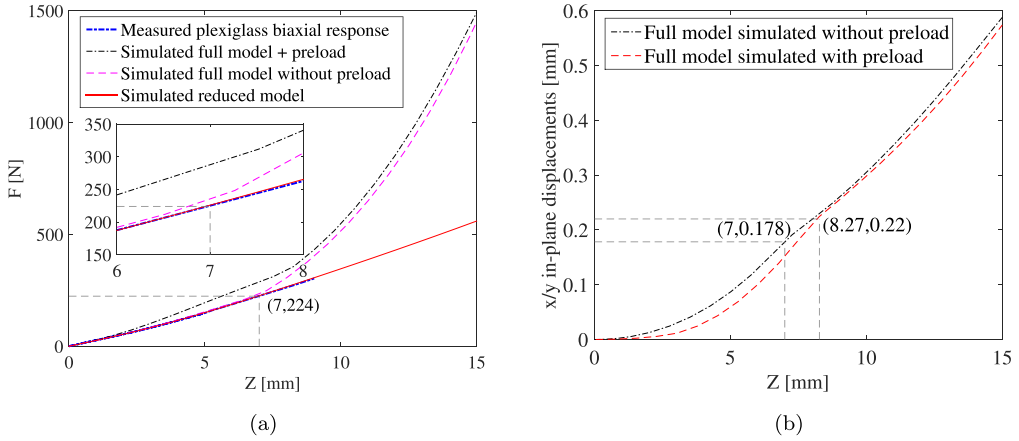

Fig. 10. Simulation of the biaxial bending model using plexiglass under different modelling assumptions: (a) $Z - F$ structural responses, (b) In-plane slippage of the plexiglass plate.

the latter comes against bolts. Accordingly, the clearance between the threaded rod and the plate plays an important role in defining the limit of usage of the biaxial model. Here, results were derived for 0.275 mm clearance. In these conditions, a maximum von Mises stress of 560 MPa corresponding to the yield limit of grade 8.8 steel, the constitutive material of fasteners, is reached at $Z = 9.52$ mm (Fig. 11). Therefore, the requirement of elasticity restrains the usage of the biaxial model to $Z = 9.52$ mm regardless of the matching between the simulated and experimental curves. Given the above, it seems appropriate to substitute the full biaxial model with a reduced model of similar specimen mesh, but where BCs would replace the set of fasteners. The two in-plane degrees of freedom of displacement and rotation

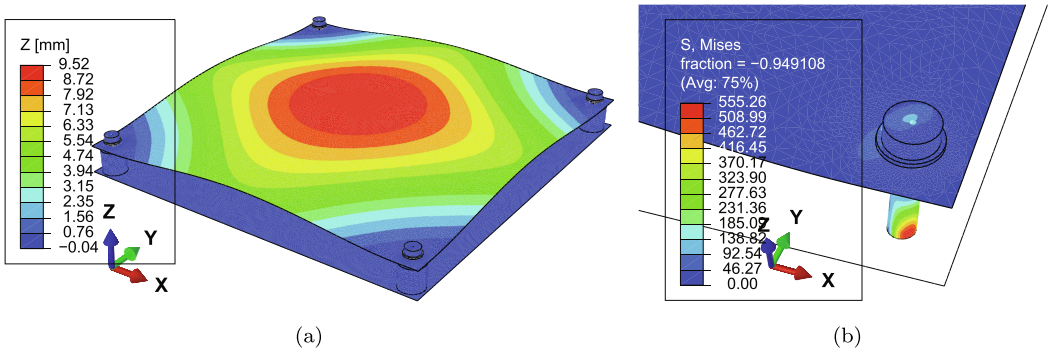

Fig. 11. Simulation of full biaxial bending model without preload force: (a) Vertical displacement response, (b) Von Mises stress state in an 8.8 grade steel bolt at $Z = 9.52$ mm.

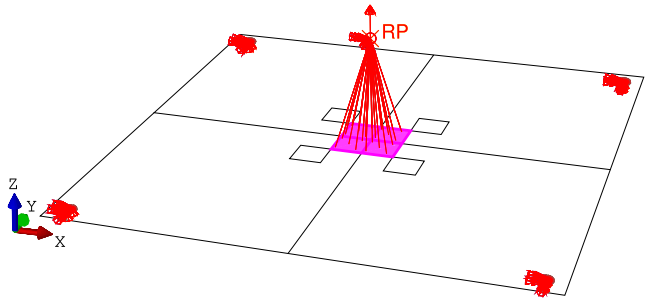

Fig. 12. Reduced biaxial model.

about z- axis of nodes of the outline of holes were freed, while the remaining degrees of freedom hold locked, which ensures specimen slippage. Fig. 10a shows that the $Z-F$ curve obtained from the reduced model agrees with its experimental and full model (without preload) counterparts until $Z = 7$ mm. The CPU-times for simulating one increment using the reduced and the full models are worth 41 and 1054 s, respectively. This led to continuing with the reduced model depicted in Fig. 12.

4. Sensitivity analyses

The forthcoming sensitivity analyses attempt to figure out the influence of the mechanical properties of E-glass material on the simulated results of the uniaxial and biaxial models. A full factorial design reported in Table 2 is considered. With minimum and maximum levels assigned to each factor, each FE model will be simulated over 32 cases. The uniaxial model was computed from 0 to 45 mm, while the biaxial model was simulated from 0 to 7 mm, its upper limit (subSection 3.3). A first sensitivity analysis considered $Y = (F, \varepsilon_c)$, the vector of responses of the uniaxial model with respect to $X = (E_l, E_c, \nu_{lc}, G_{lc}, G_{lz})$, vector of E-glass unknown mechanical properties. The average of response i, denoted by $\overline{Y}_i$, is sketched out for the minimum and maximum levels relative to each parameter X_j. It comes out that $\overline{F}$ is exclusively dependent on E_c (Fig. 13a). Fig. 13b shows the interaction between ε_c and the subset of X composed of (E_l, E_c, and ν_{lc}). Hence, the latter subset is potentially identifiable from ε_c. Nevertheless, Fig. 13b depicts that ε_c is most sensitive to ν_{lc}. A major asset of this work consists in the determination of the Poisson's ratio, difficult to obtain by standard experiments [25]. Besides, the slight difference between experimental ε_c and ε_l is in support of the material low degree of anisotropy. This permits to assert the equivalence between E_l and E_c. Thus, it could be inferred that uniaxial responses Y would identify a unique subset $X = (E_c, \nu_{lc})$. A second sensitivity study interests to the effect of E-glass mechanical properties on outputs of the biaxial model designated by $Y = (F, \varepsilon_c, \varepsilon_l, \varepsilon_d)$. Its outcomes are illustrated graphically in Fig. 14. Including additional outputs led to choose an automated sensitivity analysis through an SVD-QR method [26]. The SVD-QR operates on S sensitivity matrix defined by

$$S_{ij} = \frac{\partial Y_i}{\partial X_j} \tag{1}$$

X and Y have different units. Therefore, it becomes more advantageous to consider the relative sensitivity matrix writing

$$\widetilde{S}_{ij} = \frac{X_j \partial Y_i}{Y_i \partial X_j} \tag{2}$$

Following the SVD, S can be written as $S = U\Sigma V^t$, with U and V left and right singular vectors and Σ a matrix of singular values. The rank of Σ, denoted by r, corresponds to the number of identifiable parame-

Table 2
Full factorial design: range of factors for the E-glass material.

Factors	Unit	Minimum value	Maximum value
E_l	GPa	10	30
E_c	GPa	10	30
ν_{lc}		0.1	0.45
G_{lc}	GPa	1	10
G_{lz}	GPa	1	10

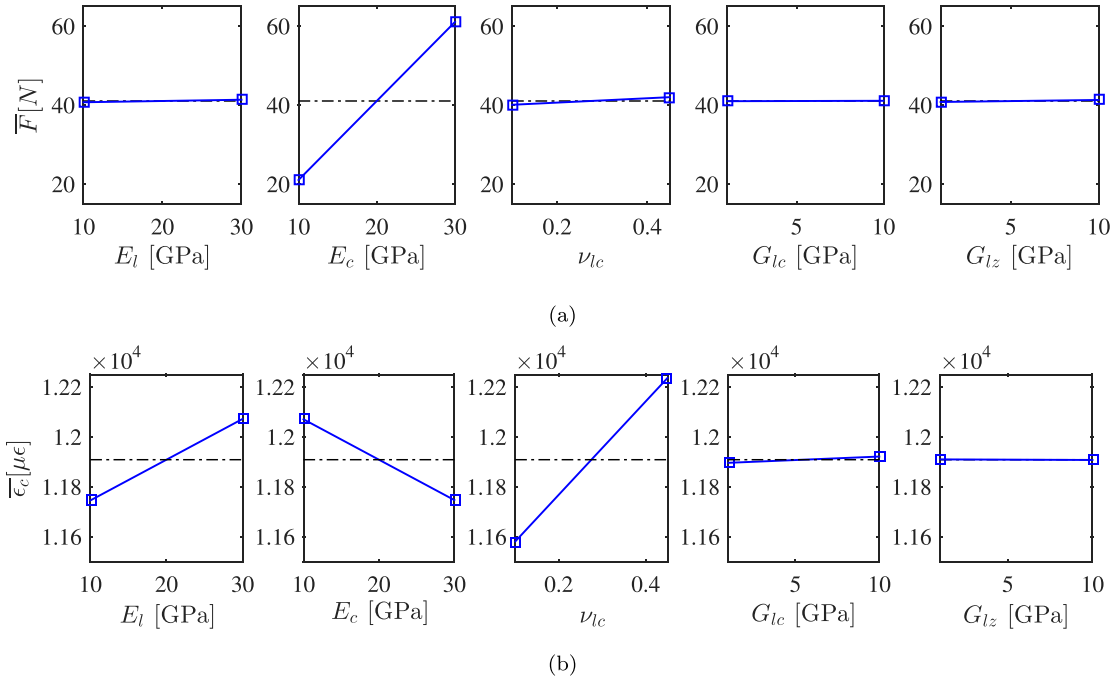

Fig. 13. Sensitivity of outputs of the uniaxial bending model to E-glass mechanical properties: (a) Main effects on the pull-up load, (b) Main effects on E-glass crosswise strain.

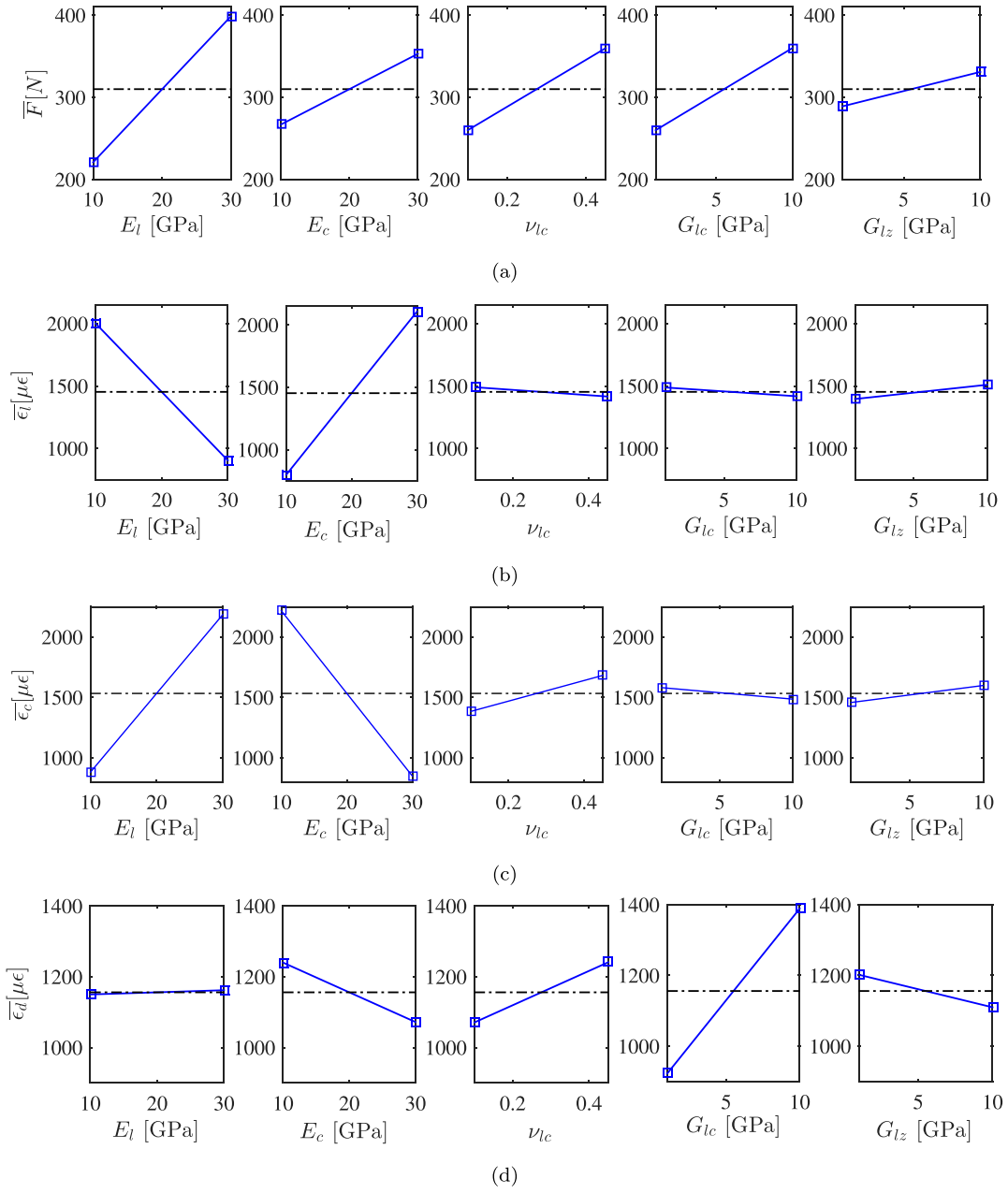

Fig. 14. Sensitivity of outputs of the biaxial bending model to E-glass mechanical properties: (a) Main effects on pull-up load, (b) Main effects on lengthwise strain, and (c) Main effects on crosswise strain, and (d) Main effects on diagonal strain.

ters from n being the size of X. This logic led to partition V in the form $V = [V_r, V_{n-r}]$. The QR decomposition is used to compute the matrix, P, according to $V_r^t P = QR$. The definitions of Q and R could be found in [26]. The matrix P permits to reorder the X vector into $\widehat{X}$ such that $\widehat{X} = P^t X$. $\widehat{X}$ vector includes r and $n-r$, namely the E-glass mechanical properties that are sensitive or not to outputs of the model, respectively. The vector of sensitive properties includes components sorted from the most to the least sensitive. The application of the SVD-QR technique to $X = (E_c, E_l, \nu_{lc}, G_{lc}, G_{lz})$ gives $r = 4$ and $\widehat{X}_r = (E_l, E_c, G_{lc}, \nu_{lc})$ sorted in order of best identification and $\widehat{X}_{n-r} = G_{lz}$, unidentifiable. It can be inferred, thus, that the biaxial bending test does not permit to determine all E-glass mechanical properties. This drives the need to invoke uniaxial test data, capable of determining E_c and ν_{lc}. So, when focusing on $X = (E_l, G_{lc}, G_{lz})$, the re-application of SDV-QR technique yields $r = 3$ and $\widehat{X}_r = (G_{lc}, E_c, G_{lz})$. The property identification procedure will be outlined in next section.

5. Updating lamina mechanical properties of the E-glass material

The updating procedure relies on an iterative change of lamina mechanical properties into uniaxial or biaxial FE models until finding the minimum mismatch, according to a cost function. The iterative updating strategy was developed in Matlab using the derivative-free method `fminsearch`. Outcomes of the sensitivity studies were conjugated to the following three-step sequential identification process:

- Step 1: identification of E_c from the minimization of $|F^s - F^e|$ fed from the uniaxial bending response data. $|.|$ stands for Euclidean norm while s and e designate the simulated and experimental responses, respectively. The updating process is tracked through the variation of E_c with respect to the number of iterations, as displayed in Fig. 15a. Simulated responses are, initially, generated

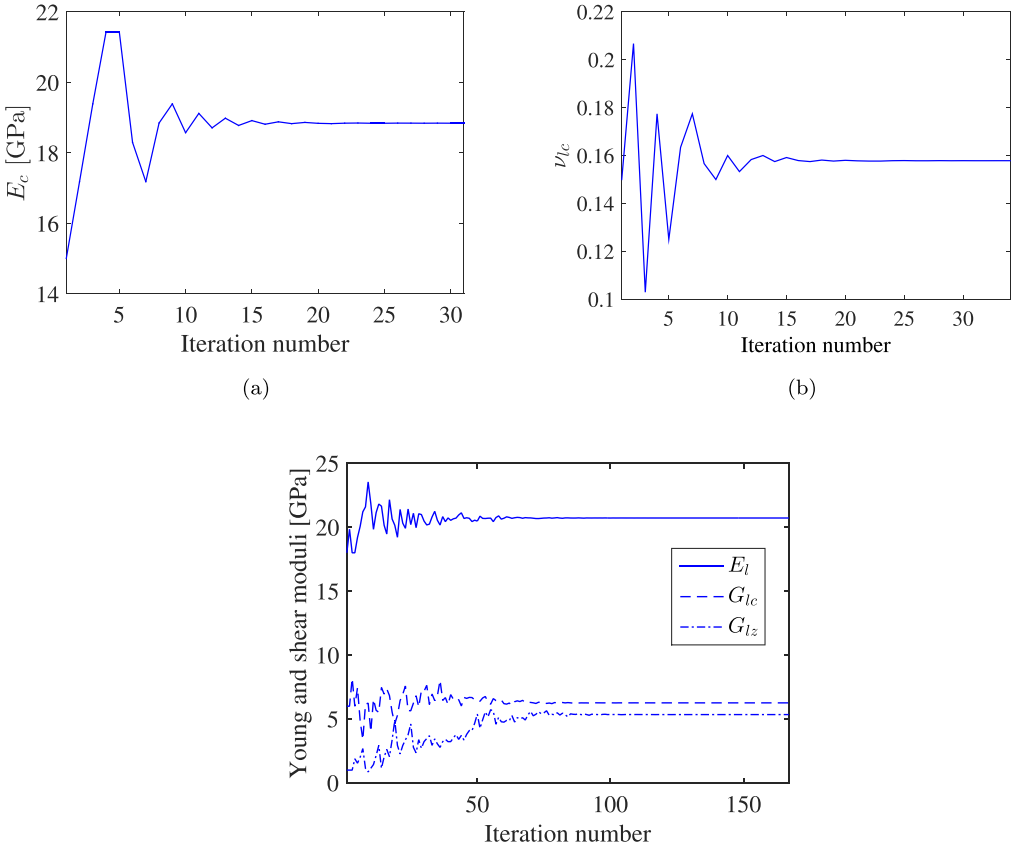

Fig. 15. The stabilization of E-glass mechanical properties upon their updating: (a) Step 1: updating of E_c, (b) Step 2: updating of ν_{lc}, and (c) Step 3: updating of E_l, G_{lc}, G_{lz}.

Table 3
Comparison of manufacturer and updated lamina mechanical properties of E-glass material.

Lamina properties	E_l	E_c	G_{lc}	$G_{lz} = G_{cz}$	ν_{lc}	ρ
Units	MPa	MPa	MPa	MPa		kg/m^3
Updated	20722	18750	6260	5343	0.158	–
NEMA brand FR4 [28]	20000	18000	–	–	0.15	1900

from an arbitrary value of Poisson's ratio and under the supposition of isotropic lamina behaviour. The convergence toward the effective E_c value was reached with less than 20 iterations for an initial value arbitrary set to 15 GPa in [10–30] GPa search interval.

- Step 2: identification of ν_{lc} based on $|\varepsilon_c^s - \varepsilon_c^e|$ provided by uniaxial bending response data within the E_c value already determined in Step 1 and the assumption of $E_c = E_l$. Fig. 15b exhibits a convergence performance similar to E_c. The standard identification

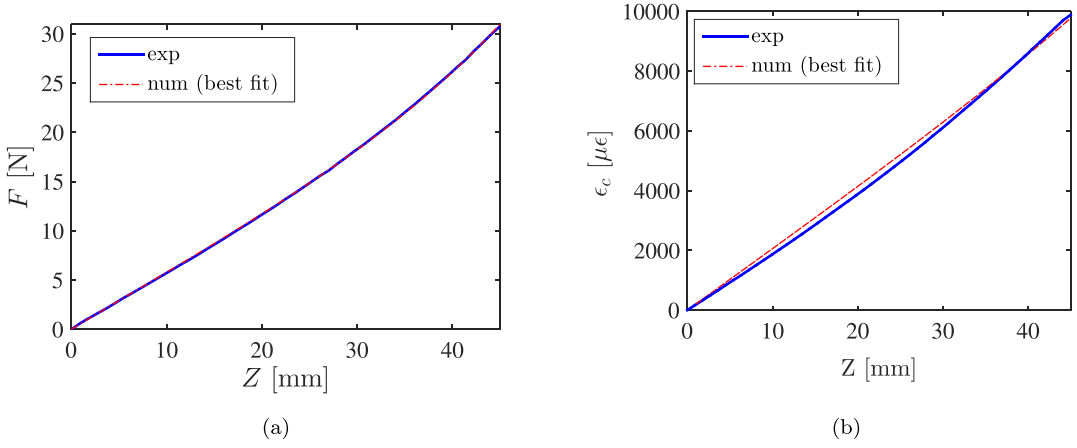

Fig. 16. Correlation between measured and simulated E-glass laminate structural responses in uniaxial bending: (a) Applied load, (b) Crosswise strain.

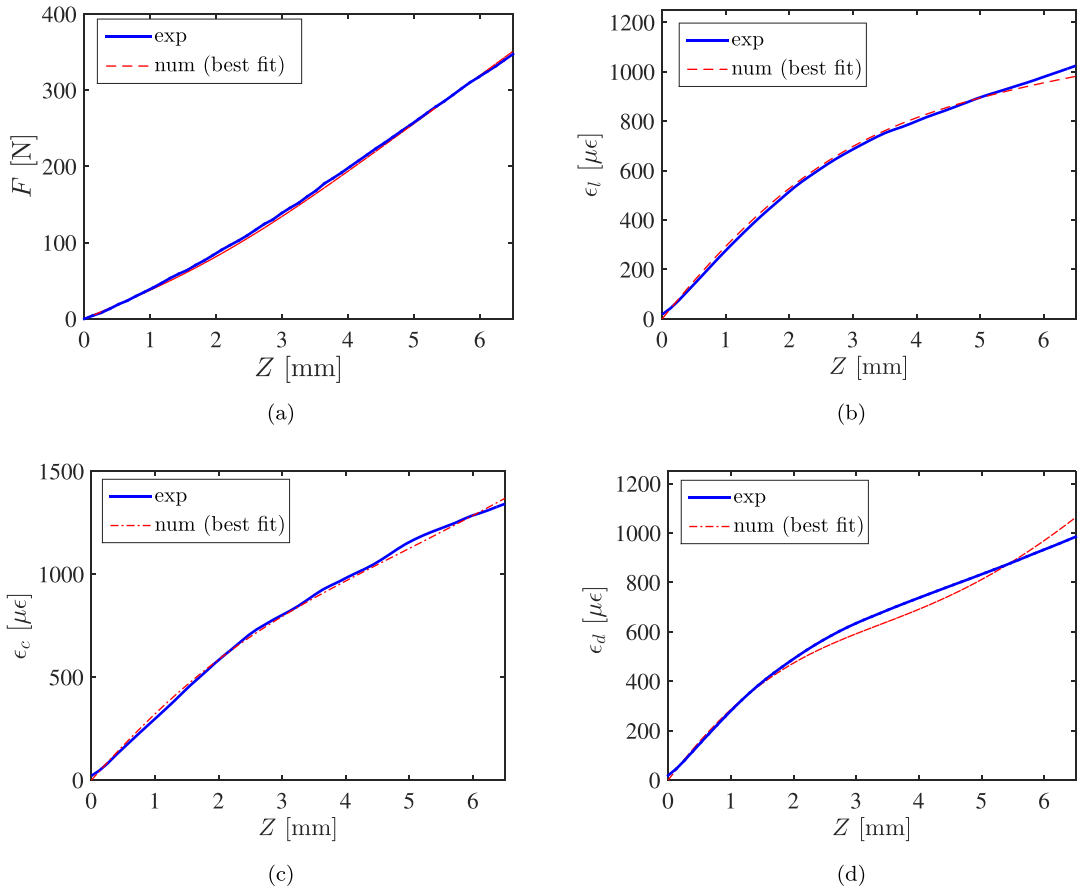

Fig. 17. Correlation between measured and simulated structural responses of E-glass laminate in biaxial bending: (a) Applied load, (b) E-glass Backplane lengthwise strain, (c) E-glass backplane crosswise strain, and (d) E-glass backplane shear strain.

method of Poisson's ratio consists of the negative ratio of the transverse strain per the axial strain along the direction of uniaxial tension [27].

- Step 3: identification in one pass of E_l, G_{lc} and G_{lz} through biaxial bending response data and setting of orthotropic behaviour for lamina. The cost function consists in the sum error $|F^s - F^e| + |\varepsilon_c^s - \varepsilon_c^e| + |\varepsilon_l^s - \varepsilon_l^e| + |\varepsilon_d^s - \varepsilon_d^e|$. The convergence stabilizes after roughly 80 iterations as obvious from Fig. 15c.

As shown in Table 3, the identified parameters greatly agree with manufacturer data. Additionally, obtaining E_l greater than E_c makes sense, knowing that warps are stiffer than wefts.

The result of identification achieved outstanding agreement between measured and simulated response data. This is apparent from Fig. 16 as concerns F and ε_c over [0–45] mm deflection in uniaxial bending. The same agreement is confirmed in [0 6.5] mm deflection range under biaxial bending as illustrated in Fig. 17 regarding $F, \varepsilon_c, \varepsilon_l$ and slightly less ε_d.

6. Conclusions

Original test models are designed in support of uniaxial and biaxial static bending tests of composite laminates, in occurrence, of E-glass material. These models ensure low cost, engineering applicability, and scalability. Beyond experiments, corresponding FE models are readily developed once boundary conditions correctly represented. This work settled the suitability of FSDT in conjunction with shell elements regarding thin laminates modelling, which can be deemed as a guideline applicable to any other arrangement. The correlation between measured and simulated structural data of test specimens subjected to bending led to the identification of the lamina mechanical properties of E-glass material. It comes out that a complete determination of these properties shall be provided imperatively by a combination of uniaxial and biaxial bending tests. The proposed updating scheme is validated through the good agreement between some updated and known manufacturer properties. Testing more specimens is, however, required to ensure the statistical consistency of the determined E-glass mechanical properties.

Declaration of Competing Interest

The authors declare that they have no known competing financial interests or personal relationships that could have appeared to influence the work reported in this paper.

Appendix A. Application of the FSDT to laminated composites

According to the FSDT, the kinematics of laminates are described by:

$$\begin{bmatrix} u \\ v \\ w \end{bmatrix} = \begin{bmatrix} u^0 \\ v^0 \\ w^0 \end{bmatrix} + z \begin{bmatrix} \phi_x \\ \phi_y \\ 0 \end{bmatrix} \tag{A.1}$$

u, v, w, ϕ_l, ϕ_c are two dimensional functions. u, v represent the in-plane displacements along x- and y-axes, respectively. w is the out-of-plane displacement which is independent of z the coordinate across thickness by supposing the inextensibility in the transverse direction

($\varepsilon_z = 0$). ϕ_x and ϕ_y describe the rotations about x- and y-axes. Note that x- and y-axes are confounded with l- and c-axes, respectively. The prime $(.)^0$ refers to the laminate mid-plane. There, strains ($\boldsymbol{\varepsilon}^0, \boldsymbol{\chi}, \boldsymbol{\gamma}$) are expressed as follows:

$$[\boldsymbol{\varepsilon}^0 \quad \boldsymbol{\chi} \quad \boldsymbol{\gamma}] = \left[\frac{\partial u}{\partial x} \quad \frac{\partial v}{\partial y} \quad \frac{\partial v}{\partial x} + \frac{\partial u}{\partial y} \frac{\partial \phi_x}{\partial x} \quad \frac{\partial \phi_y}{\partial y} \quad \frac{\partial \phi_y}{\partial x} + \frac{\partial \phi_x}{\partial y} \quad \phi_x + \frac{\partial w}{\partial x}\phi_y + \frac{\partial w}{\partial y}\right] \tag{A.2}$$

$\boldsymbol{\varepsilon}, \boldsymbol{\chi}$ and $\boldsymbol{\gamma}$ designate the in-plane strain, curvature change, and transverse shear strain vectors, respectively. That said, the constitutive equations of laminates write:

$$\begin{bmatrix} \mathbf{N} \\ \mathbf{M} \\ \mathbf{Q} \end{bmatrix} = \begin{bmatrix} \mathbf{A} & \mathbf{Ba} & \mathbf{0} \\ \mathbf{Ba} & \mathbf{B} & \mathbf{0} \\ \mathbf{0} & \mathbf{0} & \mathbf{A}_{ts} \end{bmatrix} \begin{bmatrix} \boldsymbol{\varepsilon}^0 \\ \boldsymbol{\chi} \\ \boldsymbol{\gamma} \end{bmatrix} \tag{A.3}$$

$\mathbf{N}, \mathbf{M}$ and $\mathbf{Q}$ represent the force, moment and transverse shear force resultants. $\mathbf{A}, \mathbf{Ba}$ and $\mathbf{B}$ designate the axial, bending-axial coupling, and bending stiffness matrices of the laminate, respectively. For an n-layer laminate, the former matrices become expressed in terms of in-plane laminae stiffness matrices, $\mathbf{D}_{in}^k$ ($k = 1, 2, \ldots, n$), by

$$[\mathbf{A} \quad \mathbf{Ba} \quad \mathbf{B}] = \sum_{k=1}^{n} \int_{z_k}^{z_{k+1}} \mathbf{D}_{in}^k [1 \quad z \quad z^2] dz \tag{A.4}$$

where $z_1 = -h/2, z_k$ is the z-coordinate of lower surface of the kth lamina, $z_{n+1} = h/2$ with h is the laminate thickness. In this study, the E-glass laminate is symmetric about its mid-plane as made of a stack of identical laminae. Accordingly, **Ba** takes 0 [14]. Furthermore, a unique stiffness matrix $\mathbf{D}$ could fairly replace $\mathbf{D}^k$ [13]. This is referred to as "single-layer" concept. From their manufacture process, laminae are quasi-homogeneous in the plane (plain weave fabric). Thus, xz and yz are planes of symmetry of the E-glass laminate. From this finding, the material behaviour can be considered orthotropic with $\mathbf{D}$ expressed by

$$\mathbf{D} = \begin{bmatrix} D_{11} & D_{12} & 0 & 0 & 0 \\ D_{12} & D_{22} & 0 & 0 & 0 \\ 0 & 0 & D_{66} & 0 & 0 \\ 0 & 0 & 0 & D_{44} & 0 \\ 0 & 0 & 0 & 0 & D_{55} \end{bmatrix} = \begin{bmatrix} \mathbf{D}_{in} & \mathbf{0} \\ \mathbf{0} & \mathbf{D}_{ts} \end{bmatrix} \tag{A.5}$$

Eq. (A.5) can be subdivided into an in-plane stiffness matrix, $\mathbf{D}_{in}$ defined by

$$\mathbf{D}_{in} = \begin{bmatrix} \frac{E_l}{1-\nu_{lc}\nu_{cl}} & \frac{\nu_{lc}E_c}{1-\nu_{lc}\nu_{cl}} & 0 \\ \frac{\nu_{cl}E_l}{1-\nu_{lc}\nu_{cl}} & \frac{E_c}{1-\nu_{lc}\nu_{cl}} & 0 \\ 0 & 0 & G_{lc} \end{bmatrix} \tag{A.6}$$

and a transverse stiffness matrix, $\mathbf{D}_{ts}$, given by

$$\mathbf{D}_{ts} = \begin{bmatrix} G_{lz} & 0 \\ 0 & G_{cz} \end{bmatrix} \tag{A.7}$$

$E_l, E_c, G_{lc}, G_{cz}, G_{lz}, \nu_{cl}, \nu_{lc}$ are namely the lengthwise and crosswise moduli, axial and transverse shear moduli, and the in-plane major and minor Poisson's ratios. The homogeneity of the E-glass laminate lets assume G_{lz} equivalent to G_{cz}. Furthermore, the requirement of symmetric stiffness matrix gives rise to the following restriction:

$$\nu_{lc} = \nu_{cl}\frac{E_l}{E_c} \tag{A.8}$$

Summarizing, $\mathbf{D}$ could be completely defined by five (5) mechanical properties ($E_l, E_c, G_{lc}, G_{lz}, \nu_{cl}$). The latter will make the object of FE experimental updating. Call of the single-layer concept permits to integrate Eq. (A.4) between $-h/2$ and $h/2$ which results in the following expressions of $\mathbf{A}$ and $\mathbf{B}$:

$$[\mathbf{A} \quad \mathbf{B}] = \mathbf{D}_{in}[h \quad h^3/12] \tag{A.9}$$

The sequel of this section will be devoted to define the explicit form of $\mathbf{A}_{ts}$. Call of Hooke's law and recall of $\sigma_z = 0$ lead to the following relation between stress and strain components:

$$\begin{bmatrix} \sigma_x \\ \sigma_y \\ \tau_{xy} \\ \tau_{yz} \\ \tau_{xz} \end{bmatrix} = \begin{bmatrix} \mathbf{D}_{in} & \mathbf{0} \\ \mathbf{0} & \mathbf{D}_{ts} \end{bmatrix} \begin{bmatrix} \varepsilon_x \\ \varepsilon_y \\ \varepsilon_{zy} \\ \gamma_{yz} \\ \gamma_{xz} \end{bmatrix} \tag{A.10}$$

Apart from the mid-plane, $\boldsymbol{\varepsilon}$ can be expressed in any reference plane $z = z_{x0}$ as follows:

$$\boldsymbol{\varepsilon} = \boldsymbol{\varepsilon}^0 + (z - z_{x0})\boldsymbol{\chi} \tag{A.11}$$

The combination of Eqs. (A.3) and (A.10) yields the stress state of the laminate from through-thickness integration of ($\mathbf{N}, \mathbf{M}$ and $\mathbf{Q}$). According to [29], the determination of $\mathbf{A}_{ts}$ arises from the equivalence between the laminate shear strain energy and the result of integration of shear strain energy density of laminae. This writes

$$\frac{1}{2}\mathbf{Q}^t\mathbf{A}_{ts}^{-1}\mathbf{Q} = \frac{1}{2}\sum_{k=1}^{n}\int_{z_k}^{z_{k+1}} \tau^t\mathbf{D}_{ts}^{-1}\tau \tag{A.12}$$

Retrieving $\mathbf{A}_{ts}$ under pure bending assumed in [29] fits to the present study. Under such conditions, $\mathbf{N}$ is set to 0. In-plane strain components initially brought by Eq. (A.3) become expressed by

$$\begin{cases} \boldsymbol{\chi} = \mathbf{B}^{-1}\mathbf{M} \\ \boldsymbol{\varepsilon}^0 = \mathbf{A}^{-1}\mathbf{N} = 0 \\ \boldsymbol{\varepsilon} = (z - z_{x0})\boldsymbol{\chi} \end{cases} \tag{A.13}$$

Thus, in-plane stress components can be rewritten as

$$\boldsymbol{\sigma} = \mathbf{D}_{in}\boldsymbol{\varepsilon} = \mathbf{D}_{in}(z - z_{x0})\mathbf{B}^{-1}\mathbf{M} \tag{A.14}$$

Eq. (A.9) has brought $\mathbf{B} = \frac{h^3}{12}\mathbf{D}_{in}$. Taking Eq. (A.14) into account, σ_x writes

$$\sigma_x = \frac{12(z - z_{x0})}{h^3}M_x \tag{A.15}$$

Besides it is known that

$$Q_x = \frac{\partial M_x}{\partial x} \tag{A.16}$$

According to [29], the equilibrium in bending about x-axis is governed by the following relation:

$$\frac{\partial \sigma_x}{\partial x} + \frac{\partial \tau_{xz}}{\partial z} = 0 \tag{A.17}$$

Incorporating Eqs. (A.16) and (A.15) in Eq. (A.17) yields the following

$$\frac{\partial \tau_{xz}}{\partial z} = -\frac{12(z - z_{x0})Q_x}{h^3} \tag{A.18}$$

The following boundary conditions apply in the top and bottom surfaces of the laminate

$$\begin{cases} \tau_{xz}^1 = 0 \quad \text{at} \quad z = z_1 = -\frac{h}{2} \\ \tau_{xz}^n = 0 \quad \text{at} \quad z = z_{n+1} = \frac{h}{2} \end{cases} \tag{A.19}$$

Taking into account Eqs. (A.19) in the integration of Eq. (A.18) and duplicating the same for y-axis yield the following:

$$\tau = -\frac{6}{h^3}(z^2 - h^2/4)\mathbf{Q} \tag{A.20}$$

The through-thickness integration of the right side of Eq. (A.12) using Eq. (A.20) provides the following expression of the transverse shear stiffness for the laminate

$$\mathbf{A}_{ts} = \frac{5h}{6}\mathbf{Q}_{ts} \tag{A.21}$$

5/6 is referred to as correction factor of the transverse shear stiffness. The explicit definition of all terms of the laminate stiffness matrix is very attractive in non-linear analyses where the element matrices are calculated many times [30]. This theoretical review is essential to understand the main assets of FSDT as well as its implementation into shell finite elements.

References

[1] Ullah H, Harland AR, Silberschmidt VV. Characterisation of mechanical behaviour and damage analysis of 2D woven composites under bending. Compos B Eng 2015;75:156–66.

[2] Wisnom MR, Atkinson JW. Reduction in tensile and flexural strength of unidirectional glass fibre-epoxy with increasing specimen size. Compos Struct 1997;38(1–4):405–11.

[3] ISO-178:2019. Plastics – determination of flexural properties. Standard, International Organization for Standardization; April 2019..

[4] ISO-14125:1998. Fibre-reinforced plastic composites – determination of flexural properties. Standard, International Organization for Standardization; Apr 1998.

[5] Fuchs PF, Pinter G, Tonjec M. Determination of the orthotropic material properties of individual layers of printed circuit boards. Microelectron Reliab 2012;52:2723–30.

[6] Van Paepegem W, Degrieck J. Experimental set-up for and numerical modelling of bending fatigue experiments on plain woven glass/epoxy composites. Compos Struct 51 (1): 2001; 1–8. ISSN 0263-8223..

[7] Sol H, Hua H, De Visscher J, Vantomme J, De Wilde WP. A mixed numerical/experimental technique for the nondestructive identification of the stiffness properties of fibre reinforced composite materials. NDT and E Int 1997;30 (2):85–91.

[8] Wattiaux D, Verlinden O, De Fruytier Ch. Modelling of the dynamic behaviour of electronic boards used for spatial applications. In: Proceedings of the 8th national congress of theoretical and applied mechanics. Brussels, Belgium; May 2009..

[9] Coombs CF. Printed circuits handbook. sixth ed. McGraw-Hill; 2014.

[10] Amy RA. Efficient design of spacecraft electronics to satisfy launch vibration requirements. PhD thesis, University of Southampton; 2009..

[11] Dahale M, Neale G, Lupicini R, Cascone L, McGarrigle C, Kelly J, Archer E, Harkin-Jones E, McIlhagger A. Effect of weave parameters on the mechanical properties of 3D woven glass composites. Compos Struct 2019;223.

[12] Ogihara S, Reifsnider KL. Characterization of nonlinear behavior in woven composite laminates. Appl Compos Mater 2002;9(4):249–63.

[13] Altenbach H, Becker W. Modern trends in composite laminates mechanics. Springer-Verlag Wien GmbH; 2003.

[14] Abrate S, Di Sciuva M. Equivalent single layer theories for composite and sandwich structures: a review. Compos Struct 2017;179:482–94.

[15] Christensen RM. Mechanics of composite materials. USA: John Wiley & Sons; 1979.

[16] Altenbach H. On the determination of transverse shear stiffnesses of orthotropic plates. Z Angew Math Phys 2000;51(4):629–49.

[17] Kärger L, Wetzel A, Rolfes R, Rohwer K. A three-layered sandwich element with improved transverse shear stiffness and stresses based on fsdt. Comput Struct 2006;84(13–14):843–54.

[18] ISO-25217:2009. Adhesives – determination of the mode 1 adhesive fracture energy of structural adhesive joints using double cantilever beam and tapered double cantilever beam specimens. Standard, International Organization for Standardization; May 2009..

[19] Bucalem ML, Bathe KJ. Finite element analysis of shell structures. Arch Comput Methods Eng 1997;4(1):3–61.

[20] Abaqus. Abaqus analysis user's guide, vol III. Technical report, Dassault Systemes Simulia Corp., Providence, RI, USA; 2014..

[21] Laulusa A, Bauchau OA, Choi JY, Tan VBC, Li L. Evaluation of some shear deformable shell elements. Int J Solids Struct 2006;43(17):5033–54.

[22] Evonik Industries AG. Technical information plexiglass. www.plexiglas.net, 2019 (accessed June 6, 2019)..

[23] Krolo P, Grandic D, Bulic M. The guidelines for modelling the preloading bolts in the structural connection using finite element methods. J Comput Eng 2016:2016. 4724312.

[24] Metric bolt grades and strength calculator. www.amesweb.info/Screws/Metric-Bolt-Grades-Strength.aspx; 2017 (accessed Apr 14, 2018)..

[25] ASTM D638-14. Standard Test Method for Tensile Properties of Plastics. Standard, ASTM International, West Conshohocken, PA; 2014.

[26] Olufsen MS, Ottesen JT. A practical approach to parameter estimation applied to model predicting heart rate regulation. J Math Biol 2013;67(1):39–68.

[27] ASTM D638-02a. Standard test method for tensile properties of plastics. Standard, ASTM International; November 2003..

[28] Inc The Gund Company. NEMA Grade FR4 Glass Epoxy Laminate. http://thegundcompany.com/; 2016 (accessed July 13, 2019)..

[29] Xie J, Waas AM, Rassaian M. Analytical predictions of delamination threshold load of laminated composite plates subject to flexural loading. Compos Struct 2017;179:181–94.

[30] Voyiadjis GZ, Woelke P. General non-linear finite element analysis of thick plates and shells. Int J Solids Struct 2006;43(7–8):2209–42.